Prepared for submission to JHEP MS-TP-17-06

Associated $t\bar{t}H$ production at the LHC: theoretical predictions at NLO+NNLL accuracy

Anna Kulesza,[a] **Leszek Motyka,**[b] **Tomasz Stebel**[b,c] **and Vincent Theeuwes**[d]

[a] *Institute for Theoretical Physics, WWU Münster, D-48149 Münster, Germany*
[b] *Institute of Physics, Jagellonian University, S.Łojasiewicza 11, 30-348 Kraków, Poland*
[c] *Institute of Nuclear Physics PAN, Radzikowskiego 152, 31-342 Kraków, Poland*
[d] *Department of Physics, SUNY Buffalo, 261 Fronczak Hall, Buffalo, NY 14260-1500, USA*

E-mail: anna.kulesza@uni-muenster.de, leszekm@th.if.uj.edu.pl, tomasz.stebel@uj.edu.pl, vtheeuwe@buffalo.edu

Abstract: We perform threshold resummation of soft gluon corrections to the total cross section and the invariant mass distribution for the process $pp \to t\bar{t}H$. The resummation is carried out at next-to-next-to-leading-logarithmic (NNLL) accuracy using the direct QCD Mellin space technique in the three-particle invariant mass kinematics. After presenting analytical expressions we discuss the impact of resummation on the numerical predictions for the associated Higgs boson production with top quarks at the LHC. We find that NLO+NNLL resummation leads to predictions for which the central values are remarkably stable with respect to scale variation and for which theoretical uncertainties are reduced in comparison to NLO predictions.

Keywords: QCD, Higgs boson, top quark, soft gluon resummation

arXiv:1704.03363v1 [hep-ph] 11 Apr 2017

Contents

1 Introduction **1**

2 NNLL resummation in the triple invariant mass kinematics for $2 \to 3$ processes with two massive coloured particles in the final state **3**

3 Numerical results for the $pp \to t\bar{t}H$ process at NLO+NNLL accuracy **8**

4 Summary **16**

1 Introduction

The measurement of Higgs boson production rates in the $pp \to t\bar{t}H$ process is of the central importance to the LHC research program. The process has been intensively searched for in Run 1 [1–5] and its measurement is among the highest priorities of the LHC Run 2 physics programme [6–8]. The associated production process offers a direct way to probe the strength of the top–Higgs Yukawa coupling without making any assumptions regarding its nature. As the top–Higgs Yukawa coupling is especially sensitive to the underlying physics, $t\bar{t}H$ production provides a vital test of the Standard Model (SM) and possibly a means to probe the beyond the SM physics indirectly. It is thus highly important that precise and reliable theoretical predictions are available for this process.

For these reasons, a large amount of effort has been invested to improve theoretical description of the $t\bar{t}H$ production. While the next-to-leading-order (NLO) QCD, i.e. $\mathcal{O}(\alpha_s^3\alpha)$ predictions were obtained some time ago [9, 10], they have been newly recalculated and matched to parton showers in [11–14]. In the last years, the mixed QCD-weak corrections [15] and QCD-EW corrections [16, 17] of $\mathcal{O}(\alpha_s^2\alpha^2)$ are also available. Furthermore, the NLO EW and QCD corrections to the hadronic $t\bar{t}H$ production with off-shell top and antitop quarks have been recently obtained [18, 19]. For the most part, the NLO QCD corrections are $\sim 20\%$ at the Run 2 LHC energies, whereas the size of the (electro)weak correction is more than ten times smaller. The scale uncertainty of the NLO QCD corrections is estimated to be $\sim 10\%$ [9, 10, 20].

In general, if for a given process one expects that a significant part of higher order corrections originates from emission of soft and/or collinear gluons, it is possible to improve the accuracy of theoretical predictions by employing methods of resummation. Relying on principles of factorization between various dynamical modes, they allow an all-order calculation of dominant logarithmic corrections originating from a certain kinematical limit. Supplementing fixed-order results with resummation leads not only to change in the value of the cross section but also offers a better control over the theoretical error, in particular due to cancellations of factorization scale dependence between parton distribution functions (pdfs)

and the partonic cross sections. The universality of resummation concepts warrants their applications to scattering processes with arbitrary many partons in the final state [21, 22], thus also to a class $2 \to 3$ processes and in particular the associated $t\bar{t}H$ production at the LHC.

The first step in this direction was performed by us in [23], where we presented the first calculation of the resummed total cross section for the $t\bar{t}H$ production at the next-to-leading-logarithmic (NLL) accuracy. The calculation relied on application of the traditional Mellin-space resummation formalism in the absolute threshold limit, i.e. in the limit of the partonic energy $\sqrt{\hat{s}}$ approaching the production threshold $M = 2m_t + m_H$, $\hat{s} \to M^2$, where m_t is the top quark mass and m_H is the Higgs boson mass. In [23], we have achieved an all-order improvement of the theoretical predictions by taking into account a well-defined subclass of higher order corrections. However, due to the suppression of the available 3-particle phase-space in the absolute production threshold limit, it is to be expected that the numerical impact of formally large logarithmic corrections resummed in these kinematics will be somewhat diminished and that contributions prevailing numerically might come from regions further away from the absolute threshold scale M.

Subsequently we have performed [24] resummation of NLL corrections arising in the limit of $\sqrt{\hat{s}}$ approaching the invariant mass threshold Q with $Q^2 = (p_t + p_{\bar{t}} + p_H)^2$. We have considered cross sections differential in the invariant mass Q, as well as the total cross sections obtained after integration over Q. For a $2 \to 2$ process, this type of resummation is often referred to as threshold resummation in the pair-invariant mass (PIM) kinematics. Threshold resummation can be also performed in the framework of the soft-collinear effective theory (SCET). The first application of this technique to a $2 \to 3$ process, more specifically to the process $pp \to t\bar{t}W^{\pm}$, was presented in [25]. The SCET framework was also used to obtain an approximation of the next-to-next-to-leading order (NNLO) $t\bar{t}H$ cross section and distributions [26], following from the expansion of the NNLL resummation formula. Recently, NNLL results for $t\bar{t}W$ [27], $t\bar{t}H$ [28] and $t\bar{t}Z$ [29] associated production processes appeared, based on expressing the SCET formulas in Mellin space.

In this paper, we continue the work presented in [24] and perform threshold resummation in the invariant mass limit at the NNLL accuracy using the direct QCD [30] Mellin-space approach. Compared to NLL calculations, the anomalous dimensions governing resummation need to be implemented with accuracy higher by one order. In contrast to the absolute threshold limit considered in [23], the soft anomalous dimension is a matrix in the colour space containing non-zero off-diagonal elements, thus requiring an implementation of the diagonalization procedure. We then match our NNLL cross section with the fixed-order cross section at NLO. The invariant mass kinematics also offers an opportunity to perform resummation for the differential distributions in Q.

The paper is structured as follows. In Section 2 we review threshold resummation in Mellin space, stressing the difference between the resummation in the invariant mass and the absolute threshold limits. The numerical results and their discussion is presented in Section 3, to be closed by a summary of our most important findings in Section 4.

2 NNLL resummation in the triple invariant mass kinematics for $2 \to 3$ processes with two massive coloured particles in the final state

The resummation of soft gluon corrections to the differential cross section $d\sigma_{pp\to t\bar{t}H}/dQ^2$ is performed in Mellin space, where the Mellin moments are taken w.r.t. the variable $\rho = Q^2/S$. At the partonic level, the Mellin moments for the process $ij \to klB$, where i, j denote massless coloured partons, k, l two massive quarks and B a massive colour-singlet particle, is given by

$$\frac{d\tilde{\hat{\sigma}}_{ij\to klB}}{dQ^2}(N, Q^2, \{m^2\}, \mu_{\rm F}^2, \mu_{\rm R}^2) = \int_0^1 d\hat{\rho}\, \hat{\rho}^{N-1} \frac{d\hat{\sigma}_{ij\to klB}}{dQ^2}(\hat{\rho}, Q^2, \{m^2\}, \mu_{\rm F}^2, \mu_{\rm R}^2), \tag{2.1}$$

with $\hat{\rho} = Q^2/\hat{s}$ and $\{m^2\}$ denoting all masses entering the calculations.

Taking the Mellin transform allows one to systematically treat the logarithmic terms of the form $\alpha_{\rm s}^n \left[\log^m(1-z)/(1-z)\right]_+$, with $m \leq 2n-1$ and $z = Q^2/\hat{s}$, appearing in the perturbative expansion of the partonic cross section to all orders in $\alpha_{\rm s}$. In Mellin space these logarithms turn into logarithms of the variable N, and the threshold limit $z \to 1$ corresponds to the limit $N \to \infty$.

The resummed cross section in the N-space has the form [31, 32][1]

$$\begin{aligned}\frac{d\tilde{\hat{\sigma}}^{(\rm res)}_{ij\to klB}}{dQ^2}\ (N, Q^2, \{m^2\}, \mu_{\rm F}^2, \mu_{\rm R}^2) = \\ = {\rm Tr}\left[\mathbf{H}_{ij\to klB}(Q^2, \{m^2\}, \mu_{\rm F}^2, \mu_{\rm R}^2)\mathbf{S}_{ij\to klB}(N+1, Q^2, \{m^2\}, \mu_{\rm F}^2, \mu_{\rm R}^2)\right] \\ \times\ \Delta^i(N+1, Q^2, \mu_{\rm F}^2, \mu_{\rm R}^2)\Delta^j(N+1, Q^2, \mu_{\rm F}^2, \mu_{\rm R}^2),\end{aligned} \tag{2.2}$$

where the trace is taken over colour space. The appearance of colour dependence in Eq. (2.2) is inherently related to the fact that soft radiation is coherently sensitive to the colour structure of the hard process from which it is emitted. The matrix $\mathbf{H}_{ij\to klB}$ indicates the hard-scattering contributions, absorbing the off-shell effects, projected onto the chosen colour basis. The colour matrix $\mathbf{S}_{ij\to klB}$ represents the soft wide-angle emission. The functions Δ^i and Δ^j sum the logarithmic contributions due to (soft-)collinear radiation from the incoming partons. The radiative factors are thus universal for a specific initial state parton, i.e. they depend neither on the underlying colour structure nor the process.

At LO the $t\bar{t}H$ production receives contributions from the $q\bar{q}$ and gg channels. We analyze the colour structure of the underlying processes in the s-channel colour bases, $\{c_I^q\}$ and $\{c_I^g\}$, with

$$c_{\mathbf{1}}^q = \delta^{\alpha_i\alpha_j}\delta^{\alpha_k\alpha_l}, \quad c_{\mathbf{8}}^q = T^a_{\alpha_i\alpha_j}T^a_{\alpha_k\alpha_l},$$
$$c_{\mathbf{1}}^g = \delta^{a_ia_j}\,\delta^{\alpha_k\alpha_l}, \quad c_{\mathbf{8S}}^g = T^b_{\alpha_l\alpha_k}d^{ba_ia_j}, \quad c_{\mathbf{8A}}^g = iT^b_{\alpha_l\alpha_k}f^{ba_ia_j}.$$

In the limit $N \to \infty$ the hard function $\mathbf{H}_{ij\to klB}$ carries no dependence on N and is given by the perturbative expansion

$$\mathbf{H}_{ij\to klB} = \mathbf{H}^{(0)}_{ij\to klB} + \frac{\alpha_{\rm s}}{\pi}\mathbf{H}^{(1)}_{ij\to klB} + \ldots \tag{2.3}$$

[1] In fact, the soft function $\mathbf{S}_{ij\to klB}$ as well as the radiative factors Δ^i, Δ^j are dimensionless functions of the ratios of the scales and the coupling constant at the renormalization scale. The current notation indicating dependence on the scales is introduced for brevity.

In order to perform resummation at NLL accuracy one needs to know $\mathbf{H}^{(0)}_{ij\to klB}$, whereas NNLL accuracy requires the knowledge of the $\mathbf{H}^{(1)}_{ij\to klB}$ coefficient.

The soft function, on the other hand, resums logarithms of N at the rate of one power of the logarithm per power of the strong coupling. These single logarithms due to the soft emission can be confronted with double logarithms due to soft and collinear emissions resummed by the jet factors Δ^i and Δ^j. As a dimensionless function, $\mathbf{S}_{ij\to klB}$ depends only on the ratio of the scales. At the same time, the dependence on N enters only via Q/N [33], making $\mathbf{S}_{ij\to klB}$ dependent on the ratio $Q/(N\mu_{\rm F})$. The soft function is given by a solution of the renormalization group equation [31, 34] and has the form

$$\begin{aligned}\mathbf{S}_{ij\to klB}(N,Q^2,\{m^2\},\mu_{\rm F}^2,\mu_{\rm R}^2) = \bar{\mathbf{U}}_{ij\to klB}(N,Q^2,\{m^2\},\mu_{\rm F}^2,\mu_{\rm R}^2)\,\tilde{\mathbf{S}}_{ij\to klB}(\alpha_{\rm s}(Q^2/\bar{N}^2))\\ \times\,\mathbf{U}_{ij\to klB}(N,Q^2,\{m^2\},\mu_{\rm F}^2,\mu_{\rm R}^2),\end{aligned} \tag{2.4}$$

where $\tilde{\mathbf{S}}_{ij\to klB}$ plays a role of a boundary condition and is obtained by taking $\mathbf{S}_{ij\to klB}$ at $Q^2/(\bar{N}^2\mu_{\rm F}^2)=1$ with $\bar{N}=Ne^{\gamma_{\rm E}}$ and $\gamma_{\rm E}$ denoting the Euler constant. It is a purely eikonal function [31, 34, 35] and can be calculated perturbatively

$$\tilde{\mathbf{S}}_{ij\to klB} = \tilde{\mathbf{S}}^{(0)}_{ij\to klB} + \frac{\alpha_{\rm s}}{\pi}\tilde{\mathbf{S}}^{(1)}_{ij\to klB} + \dots \tag{2.5}$$

At the lowest order the colour matrix is given by:

$$\left(\tilde{\mathbf{S}}^{(0)}_{ij\to kl}\right)_{IJ} = \mathrm{Tr}\left[c_I^\dagger c_J\right]. \tag{2.6}$$

Similarly to the hard function, knowledge of $\mathbf{S}^{(0)}_{ij\to klB}$ is required in order to perform resummation at NLL accuracy and a result for $\mathbf{S}^{(1)}_{ij\to klB}$ at the NNLL accuracy. The scale of $\alpha_{\rm s}$ in $\tilde{\mathbf{S}}_{ij\to kl}$, equal to $Q^2/\bar{N}^2$, results in an order $\alpha_{\rm s}^2\log\bar{N}$ term if we expand $\tilde{\mathbf{S}}_{ij\to kl}$ in $\alpha_{\rm s}(\mu_{\rm R}^2)$. This is a NNLL effect that we resum by adding an appropriate term to the two-loop soft anomalous dimension matrix.

The soft function evolution matrices $\bar{\mathbf{U}}_{ij\to klB}$, $\mathbf{U}_{ij\to klB}$ contain logarithmic enhancements due to soft wide-angle emissions [31, 36][2]

$$\begin{aligned}\bar{\mathbf{U}}_{ij\to klB}\left(N,Q^2,\{m^2\},\mu_{\rm F}^2,\mu_{\rm R}^2\right) &= \bar{\rm P}\exp\left[\int_{\mu_{\rm F}}^{Q/\bar{N}}\frac{dq}{q}\boldsymbol{\Gamma}^\dagger_{ij\to klB}\left(\alpha_{\rm s}\left(q^2\right)\right)\right],\\ \mathbf{U}_{ij\to klB}\left(N,Q^2,\{m^2\},\mu_{\rm F}^2,\mu_{\rm R}^2\right) &= {\rm P}\exp\left[\int_{\mu_{\rm F}}^{Q/\bar{N}}\frac{dq}{q}\boldsymbol{\Gamma}_{ij\to klB}\left(\alpha_{\rm s}\left(q^2\right)\right)\right],\end{aligned} \tag{2.7}$$

where P and $\bar{\rm P}$ denote the path- and reverse path-ordering in the variable q, respectively. The soft anomalous dimension $\boldsymbol{\Gamma}_{ij\to klB}$ is a perturbative function in $\alpha_{\rm s}$:

$$\boldsymbol{\Gamma}_{ij\to klB}\left(\alpha_{\rm s}\right) = \left[\left(\frac{\alpha_{\rm s}}{\pi}\right)\boldsymbol{\Gamma}^{(1)}_{ij\to klB} + \left(\frac{\alpha_{\rm s}}{\pi}\right)^2\boldsymbol{\Gamma}^{(2)}_{ij\to klB} + \dots\right]. \tag{2.8}$$

[2]For simplicity, the argument dependence of the soft anomalous dimension on the mass scales is suppressed in Eq. (2.7).

In order to perform resummation at NLL accuracy we need to know $\mathbf{\Gamma}^{(1)}_{ij\to klB}$, whereas NNLL accuracy requires including $\mathbf{\Gamma}^{(2)}_{ij\to klB}$. The one-loop soft anomalous dimension for the process $ij \to klB$ with k, l being heavy quarks can be found e.g. in [23]. The two-loop contributions to the soft anomalous dimension were calculated in [37, 38][3]. In the triple-invariant mass (TIM) kinematics, the soft anomalous dimension matrix in general contains off-diagonal terms, thus complicating the evaluation of the resummed cross section. At NNLL additional difficulty arises because of non-commutativity of $\mathbf{\Gamma}^{(1)}_{ij\to klB}$ and $\mathbf{\Gamma}^{(2)}_{ij\to klB}$ matrices.

We make use of the method of [31] in order to diagonalize the one-loop soft anomalous dimension matrix. Denoting the diagonalization matrix for $\mathbf{\Gamma}^{(1)}_{ij\to klB}$ by $\mathbf{R}$ we have

$$\mathbf{\Gamma}^{(1)}_{R} = \mathbf{R}^{-1}\mathbf{\Gamma}^{(1)}_{ij\to klB}\mathbf{R}, \tag{2.9}$$

where the diagonalized matrix is given by eigenvalues $\lambda^{(1)}_I$ of $\mathbf{\Gamma}^{(1)}_{ij\to klB}$

$$\mathbf{\Gamma}^{(1)}_{R,IJ} = \lambda^{(1)}_I \delta_{IJ},$$

and can be also written as $\mathbf{\Gamma}^{(1)}_{R} = \left[\overrightarrow{\lambda}^{(1)}\right]_D$ with $\overrightarrow{\lambda}^{(1)} = \left\{\lambda^{(1)}_1, \ldots, \lambda^{(1)}_D\right\}$. The other matrices are transformed as:

$$\begin{aligned}
\mathbf{\Gamma}^{(2)}_{R} &= \mathbf{R}^{-1}\,\mathbf{\Gamma}^{(2)}_{ij\to klB}\,\mathbf{R}, \\
\mathbf{H}_{R} &= \mathbf{R}^{-1}\,\mathbf{H}_{ij\to klB}\,\left(\mathbf{R}^{-1}\right)^{\dagger}, \\
\tilde{\mathbf{S}}_{R} &= \mathbf{R}^{\dagger}\,\tilde{\mathbf{S}}_{ij\to klB}\,\mathbf{R}.
\end{aligned} \tag{2.10}$$

At NLL accuracy, by changing the colour basis to the one in which $\mathbf{\Gamma}^{(1)}_{ij\to klB}$ is diagonal, the path ordered exponentials in Eq. (2.4) reduce to sum over simple exponentials. At NNLL accuracy, to recast the path ordered exponential of the soft anomalous dimension matrix in a form containing simple exponential functions, we make use of a technique detailed in e.g. [41, 42] resulting in

$$\mathbf{U}_R(N, Q^2, \{m^2\}, \mu_{\rm F}^2, \mu_{\rm R}^2) = \left(\mathbf{1} + \frac{\alpha_{\rm s}\left(Q^2/\bar{N}^2\right)}{\pi}\mathbf{K}\right)\left[\left(\frac{\alpha_{\rm s}\left(\mu_{\rm F}^2\right)}{\alpha_{\rm s}\left(Q^2/\bar{N}^2\right)}\right)^{\frac{\overrightarrow{\lambda}^{(1)}}{2\pi b_0}}\right]_D\left(\mathbf{1} - \frac{\alpha_{\rm s}\left(\mu_{\rm F}^2\right)}{\pi}\mathbf{K}\right), \tag{2.11}$$

with the subscript D indicating a diagonal matrix. The matrix $\mathbf{K}$ is given by

$$K_{IJ} = \delta_{IJ}\lambda^{(1)}_I\frac{b_1}{2b_0^2} - \frac{\left(\mathbf{\Gamma}^{(2)}_R\right)_{IJ}}{2\pi b_0 + \lambda^{(1)}_I - \lambda^{(1)}_J}, \tag{2.12}$$

where b_0 and b_1 are the first two coefficients of expansion $\beta_{\rm QCD}$ in $\alpha_{\rm s}$:

$$b_0 = \frac{11C_{\rm A} - 4n_{\rm f}T_{\rm R}}{12\pi}, \tag{2.13}$$

$$b_1 = \frac{17C_{\rm A}^2 - n_{\rm f}T_{\rm R}\left(10C_{\rm A} + 6C_{\rm F}\right)}{24\pi^2}. \tag{2.14}$$

[3]Note that while using the radiative factors as given in [39, 40], we need to subtract the collinear soft radiation already included in Δ^i, Δ^j from the eikonal cross section used to calculate the soft function.

In our calculation we set $n_{\rm f} = 5$.

In the diagonal basis of the one-loop soft anomalous dimension, up to NNLL accuracy Eq. (2.2) can be written as

$$\begin{aligned}\frac{d\tilde{\hat{\sigma}}^{(\rm NNLL)}_{ij\to klB}}{dQ^2}\ (N, Q^2, \{m^2\}, \mu_{\rm F}^2, \mu_{\rm R}^2) &= \left(1 + \frac{\alpha_{\rm s}(\mu_{\rm R}^2)}{\pi} \mathcal{C}^{(1)}_{ij\to klB}(Q^2, \{m^2\}, \mu_{\rm F}^2, \mu_{\rm R}^2)\right) \\ &\times {\rm Tr}\left[\boldsymbol{\sigma}_R^{(0)}(Q^2, \{m^2\}, \mu_{\rm R}^2)\, \bar{\mathbf{U}}_R(N+1, Q^2, \{m^2\}, Q^2, \mu_{\rm R}^2)\, \tilde{\mathbf{S}}_R^{(0)}\right. \\ &\times \left.\mathbf{U}_R(N+1, Q^2, \{m^2\}, Q^2, \mu_{\rm R}^2)\right] \Delta^i(N+1, Q^2, \mu_{\rm F}^2, \mu_{\rm R}^2) \Delta^j(N+1, Q^2, \mu_{\rm F}^2, \mu_{\rm R}^2).\end{aligned} \tag{2.15}$$

In the above equation, the factor $\boldsymbol{\sigma}_R^{(0)}$ stands for the Born cross section projected onto the R-colour basis. Furthermore, all $\mathcal{O}(\alpha_{\rm s})$ corrections constant in N at $N \to \infty$ are collected in a matching coefficient $\mathcal{C}^{(1)}_{ij\to klB}$. This coefficient takes into account non-logarithmic contributions coming from the hard function $\mathbf{H}_R^{(1)}$, soft function $\tilde{\mathbf{S}}_R^{(1)}$, and the soft matrix evolution factors $\bar{\mathbf{U}}_R$ and $\mathbf{U}_R$ (corresponding to contributions from evolution between $\mu_{\rm F}$ and Q), expanded up to $\mathcal{O}(\alpha_{\rm s})$. In general such a matching coefficient would also be given by a colour matrix. However, in what follows, we approximate it with a colour averaged quantity. This coefficient is obtained at all points of the phase space by combining the virtual corrections and the infrared-limit of the real corrections [43] using the method initially proposed in [44, 45].

Substituting the expression for the running coupling, we obtain up to NNLL accuracy for the soft matrix evolution factors in Eq. (2.15)

$$\mathbf{U}_R(N, Q^2, \{m^2\}, Q^2, \mu_{\rm R}^2) = \left(\mathbf{1} + \frac{\alpha_{\rm s}(\mu_{\rm R}^2)}{\pi(1-2\lambda)}\mathbf{K}\right)\left[e^{g_s(N)\vec{\lambda}^{(1)}}\right]_D\left(\mathbf{1} - \frac{\alpha_{\rm s}(\mu_{\rm R}^2)}{\pi}\,\mathbf{K}\right), \tag{2.16}$$

$$\bar{\mathbf{U}}_R(N, Q^2, \{m^2\}, Q^2, \mu_{\rm R}^2) = \left(\mathbf{1} - \frac{\alpha_{\rm s}(\mu_{\rm R}^2)}{\pi}\,\mathbf{K}^\dagger\right)\left[e^{g_s(N)\left(\vec{\lambda}^{(1)}\right)^*}\right]_D\left(\mathbf{1} + \frac{\alpha_{\rm s}(\mu_{\rm R}^2)}{\pi(1-2\lambda)}\mathbf{K}^\dagger\right), \tag{2.17}$$

where:

$$\begin{aligned}g_s(N) = \frac{1}{2\pi b_0}\left\{\log(1-2\lambda) + \alpha_{\rm s}(\mu_{\rm R}^2)\left[\frac{b_1}{b_0}\frac{\log(1-2\lambda)}{1-2\lambda} - 2\gamma_{\rm E} b_0 \frac{2\lambda}{1-2\lambda}\right.\right. \\ \left.\left. + b_0 \log\left(\frac{Q^2}{\mu_{\rm R}^2}\right)\frac{2\lambda}{1-2\lambda}\right]\right\},\end{aligned} \tag{2.18}$$

where the constant contributions have been shifted to the matching coefficient eliminating the $\mu_{\rm F}$ dependence and

$$\lambda = \alpha_{\rm s}(\mu_{\rm R}^2) b_0 \log N. \tag{2.19}$$

The other factors contributing to the resummation of logarithms, i.e. the radiative factors for the incoming partons, Δ^i and Δ^j are widely known. The results at NLL accuracy can be found for example in [39, 46] and at the NNLL level in [40].

As already noted, at NLL accuracy, by changing the colour basis to R-basis, the path ordered exponentials in Eq. (2.4) reduce to sum over simple exponentials. Equivalently,

the NLL accuracy can be obtained by neglecting terms suppressed by a factor of α_s in Eqs. (2.16), (2.17) and (2.18). This results in the soft matrix evolution factors turning into exponential functions for the eigenvalues of the soft anomalous dimension matrix. At NLL, it is also enough to only know the LO contributions to the hard and soft function, what results in the following expression for the resummed cross section in the Mellin space

$$\begin{aligned}\frac{d\tilde{\tilde{\sigma}}^{(\mathrm{NLL})}_{ij\to klB}}{dQ^2}\ (N,Q^2,\{m^2\},\mu_\mathrm{F}^2,\mu_\mathrm{R}^2) &= \boldsymbol{\sigma}^{(0)}_{R,IJ}(Q^2,\{m^2\},\mu_\mathrm{R}^2)\,\tilde{\mathbf{S}}^{(0)}_{R,JI}\\ &\times\ \Delta^i(N+1,Q^2,\mu_\mathrm{F}^2,\mu_\mathrm{R}^2)\Delta^j(N+1,Q^2,\mu_\mathrm{F}^2,\mu_\mathrm{R}^2)\\ &\times\ \exp\left[\frac{\log(1-2\lambda)}{2\pi b_0}\left(\left(\lambda_J^{(1)}\right)^*+\lambda_I^{(1)}\right)\right],\end{aligned} \tag{2.20}$$

where the color indices I and J are implicitly summed over. The incoming parton radiative factors Δ_i are now considered only at NLL accuracy.

In order to improve the accuracy of the numerical approximation provided by resummation, it is customary to include up to $\mathcal{O}(\alpha_s)$ terms constant in N in the limit $N\to\infty$ by introducing the one-loop matching coefficient $\mathcal{C}^{(1)}_{ij\to klB}$ in the same way as at NNLL, leading to

$$\begin{aligned}\frac{d\tilde{\tilde{\sigma}}^{(\mathrm{NLL\ w\ }\mathcal{C})}_{ij\to klB}}{dQ^2}\ (N,Q^2,\{m^2\},\mu_\mathrm{F}^2,\mu_\mathrm{R}^2) &= \left(1+\frac{\alpha_s(\mu_\mathrm{R}^2)}{\pi}\mathcal{C}^{(1)}_{ij\to klB}(Q^2,\{m^2\},\mu_\mathrm{F}^2,\mu_\mathrm{R}^2)\right)\\ &\times\ \boldsymbol{\sigma}^{(0)}_{R,IJ}(Q^2,\{m^2\},\mu_\mathrm{R}^2)\,\tilde{\mathbf{S}}^{(0)}_{R,JI}\Delta^i(N+1,Q^2,\mu_\mathrm{F}^2,\mu_\mathrm{R}^2)\Delta^j(N+1,Q^2,\mu_\mathrm{F}^2,\mu_\mathrm{R}^2)\\ &\times\ \exp\left[\frac{\log(1-2\lambda)}{2\pi b_0}\left(\left(\lambda_J^{(1)}\right)^*+\lambda_I^{(1)}\right)\right].\end{aligned} \tag{2.21}$$

The resummation-improved cross sections for the $pp\to t\bar{t}H$ process are obtained through matching the resummed expressions with the full NLO cross sections

$$\begin{aligned}\frac{d\sigma^{(\mathrm{matched})}_{h_1h_2\to klB}}{dQ^2}(Q^2,\{m^2\},\mu_\mathrm{F}^2,\mu_\mathrm{R}^2) &= \frac{d\sigma^{(\mathrm{NLO})}_{h_1h_2\to klB}}{dQ^2}(Q^2,\{m^2\},\mu_\mathrm{F}^2,\mu_\mathrm{R}^2)\\ &+\ \frac{d\sigma^{(\mathrm{res-exp})}_{h_1h_2\to klB}}{dQ^2}(Q^2,\{m^2\},\mu_\mathrm{F}^2,\mu_\mathrm{R}^2)\end{aligned} \tag{2.22}$$

with

$$\begin{aligned}\frac{d\sigma^{(\mathrm{res-exp})}_{h_1h_2\to klB}}{dQ^2}(Q^2,\{m^2\},\mu_\mathrm{F}^2,\mu_\mathrm{R}^2) &= \sum_{i,j}\int_\mathsf{C}\frac{dN}{2\pi i}\,\rho^{-N}f^{(N+1)}_{i/h_1}(\mu_\mathrm{F}^2)\,f^{(N+1)}_{j/h_2}(\mu_\mathrm{F}^2)\\ \times\left[\frac{d\tilde{\tilde{\sigma}}^{(\mathrm{res})}_{ij\to klB}}{dQ^2}(N,Q^2,\{m^2\},\mu_\mathrm{F}^2,\mu_\mathrm{R}^2)\right.&\left.-\frac{d\tilde{\tilde{\sigma}}^{(\mathrm{res})}_{ij\to klB}}{dQ^2}(N,Q^2,\{m^2\},\mu_\mathrm{F}^2,\mu_\mathrm{R}^2)\big|_{(\mathrm{NLO})}\right],\end{aligned} \tag{2.23}$$

where "matched" can stand for "NLO+NNLL", "NLO+NLL" or "NLO+NLL w $\mathcal{C}$" and "res" for "NNLL", "NLL" or "NLL w $\mathcal{C}$", correspondingly. The inclusive cross section is obtained by integrating the invariant mass distribution given in Eq. (2.15) over Q^2 and

$\hat{\sigma}^{(\mathrm{res})}_{ij\to klB}(N,\mu_{\mathrm{F}}^2,\mu_{\mathrm{R}}^2)\,|_{(\mathrm{NLO})}$ represents its perturbative expansion truncated at NLO. The moments of the parton distribution functions (pdf) $f_{i/h}(x,\mu_{\mathrm{F}}^2)$ are defined in the standard way

$$f_{i/h}^{(N)}(\mu_{\mathrm{F}}^2) \equiv \int_0^1 dx\, x^{N-1} f_{i/h}(x,\mu_{\mathrm{F}}^2).$$

The inverse Mellin transform (2.23) is evaluated numerically using a contour C in the complex-N space according to the "Minimal Prescription" method developed in Ref. [39].

3 Numerical results for the $pp \to t\bar{t}H$ process at NLO+NNLL accuracy

In this section we present and discuss our state-of-the-art NLO+NNLL predictions for the $t\bar{t}H$ production process at the LHC for two collision energies $\sqrt{S} = 13$ TeV and $\sqrt{S} = 14$ TeV. The results for the total cross section which we present below are obtained by integrating out the invariant mass distribution over invariant mass Q. The distribution in Q undergoes resummation of soft gluon corrections in the threshold limit $\hat{s} \to Q^2$, i.e. in the invariant mass kinematics. This approach is different from directly resumming corrections to the total cross section in the absolute threshold limit $\hat{s} \to M^2$, which we performed in [23]. Numerical results involving resummation are obtained using two independently developed in-house computer codes. Apart from NLL and NNLL predictions matched to NLO according to Eq. (2.22), we also show the NLL predictions supplemented with the first-order hard-matching coefficients $\mathcal{C}^{(1)}_{ij\to klB}$, also matched to NLO.

In the phenomenological analysis we use $m_t = 173$ GeV and $m_H = 125$ GeV. The NLO cross section is calculated using the aMC@NLO code [47]. We perform the current analysis employing PDF4LHC15_100 sets [48] and use the corresponding values of α_{s}. In particular, for the NLO+NLL predictions we use the NLO sets, whereas the NLO+NNLL predictions are calculated with NNLO sets.

We present most of our analysis for two choices of the central values of the renormalization and factorization scales: $\mu_0 = \mu_{\mathrm{F},0} = \mu_{\mathrm{R},0} = Q$ and $\mu_0 = \mu_{\mathrm{F},0} = \mu_{\mathrm{R},0} = M/2$. The former choice is motivated by invariant mass Q being the natural scale for the invariant mass kinematics used in resummation. The latter choice of the scale is often made in the NLO calculations of the total cross section reported in the literature, see e.g. [20]. By studying results for these two relatively distant scales, we aim to cover a span of scale choices relevant in the problem. The theoretical error due to scale variation is calculated using the so called 7-point method, where the minimum and maximum values obtained with $(\mu_{\mathrm{F}}/\mu_0, \mu_{\mathrm{R}}/\mu_0) = (0.5,0.5),(0.5,1),(1,0.5),(1,1),(1,2),(2,1),(2,2)$ are considered. For reasons of technical simplicity, the pdf error is calculated for the NLO predictions, however we expect that adding the soft gluon corrections only minimally influences the value of the pdf error.

As discussed in the previous section for the evaluation of the first-order hard matching coefficients $\mathcal{C}^{(1)}_{ij\to klB}$ in equation (2.15) we need to know virtual corrections to the process. We extract them numerically using the publicly available POWHEG implementation of the $t\bar{t}H$ process [14]. For this purpose we further develop techniques employed in [23], as now we also need to know the kinematical dependence of virtual corrections. These

partial results were then cross-checked using the standalone MadLoop implementation in aMC@NLO [11]. The implementation of the virtual corrections to $ij \to t\bar{t}H$ in POWHEG and in aMC@NLO does not allow for their separate extraction in each colour channel. Instead, we extract the value which contributes to the coefficient $\mathcal{C}^{(1)}_{ij\to klB}$ averaged over colour channels. Note however, that $\mathcal{C}^{(1)}_{ij\to klB}$ in equation (2.15), valid at NNLL accuracy, is averaged over colour channels. The effects of colour mixing between $\mathbf{H}_{ij\to klB}$ and $\mathbf{S}_{ij\to klB}$ functions in equation (2.2) enter only[4] at N^{3}LL, as they involve soft wide-angle exchanges combined with non-logarithmic $\mathcal{O}(\alpha_s)$ corrections.

We begin the discussion of numerical results by analyzing how well the full NLO result for the total cross section is approximated by the expansion of the resummed cross section up to the same accuracy in α_s as in NLO. It was first pointed out in [25] in the context of the $t\bar{t}W$ production and then later in [26] for the $t\bar{t}H$ process that the qg production channel carries a relatively large numerical significance, especially in relation to the scale uncertainty. This is due to the fact that a non-zero contribution from the qg channel appears first at NLO, i.e. it is subleading w.r.t. contributions from the $q\bar{q}$ and gg channels. Correspondingly, no resummation is performed for this channel and it enters the matched resummation-improved formula Eq. (2.22) only through a fixed order contribution at NLO. It is then clear that in order to estimate how much of the NLO result is constituted by the terms accounted for in the resummed expression, Eq. (2.15), its expansion should not be directly compared with full NLO but with NLO cross section without a contribution from the qg channel. We obtain the latter result by running the numerical code of [9]. Its comparison with the expansion of the resummed expression in Eq. (2.15) up to NLO accuracy in α_s as a function of the scale $\mu = \mu_F = \mu_R$ is shown in Figure 1 for $\sqrt{S} = 14$ TeV and two choices of the central scale $\mu_0 = Q$ and $\mu_0 = M/2$. While in both cases the expansion of the resummed cross section differs significantly from the full NLO, it indeed very well approximates the NLO result with the qg channel contribution subtracted. Such a very good agreement lets us conclude that the NNLL resummed formula will indeed take into account a prevailing part of the logarithmic contributions from the $q\bar{q}$ and gg channels to all orders in α_s.[5] Additionally, the observed agreement further assures us that using the approximation of the singlet and octet hard-matching coefficients in the gg channel by their colour channel-weighted average instead of exact results has no considerable effect on the numerical predictions.

Our numerical predictions for the total cross sections at $\sqrt{S} = 13$ TeV and $\sqrt{S} = 14$ TeV are shown in Table 1. We report results obtained with our default scale choice $\mu_0 = Q$ as well as the fixed scale $\mu_0 = M/2$. Additionally, we also provide results for the 'in-between' choice of $\mu_0 = Q/2$. While for these choices of central scale the NLO results vary by 20 %, the variation[6] reduces as the accuracy of resumation increases. In particular, the

[4] The lowest order at which this approximation plays a rôle is the $\alpha_s^2 \log(N)$ correction to the leading order cross section.

[5] Although the expansion and the NLO results w/o the qg channel contribution agree very well at this level of accuracy in α_s, since we do not know the second-order hard-matching coefficients we cannot expect an equally good approximation of the NNLO result by the expansion of the NNLL formula.

[6] The value of 10% scale error often quoted in the literature relates to a variation by factors of 0.5 and

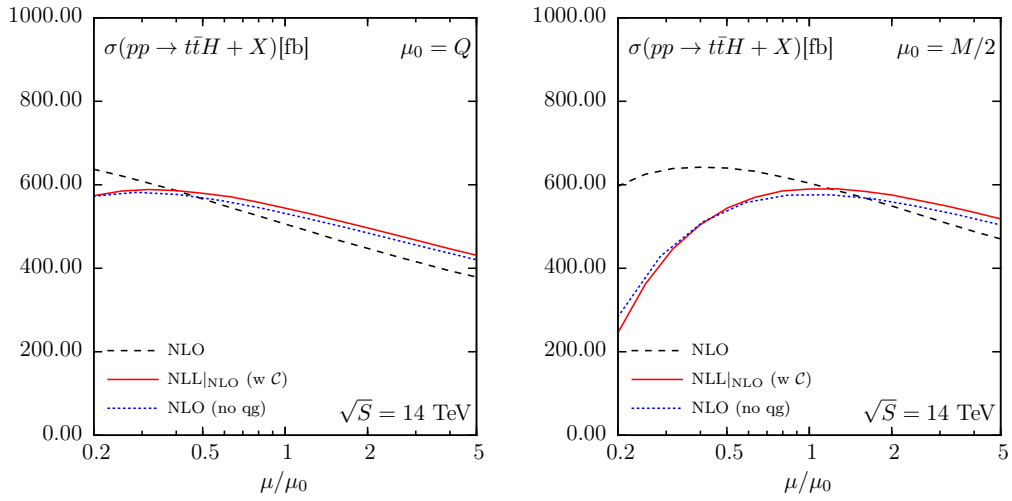

Figure 1. Comparison between the expansion of the resummed expression Eq. 2.15 up to NLO accuracy in α_s, the full NLO result and the NLO result without the qg channel contribution as a function of the scale $\mu = \mu_F = \mu_R$.

$\sqrt{S}$ [TeV]	μ_0	NLO [fb]	NLO+NLL[fb]	NLO+NLL with $\mathcal{C}$ [fb]	NLO+NNLL[fb]
13	Q	$418^{+11.9\%}_{-11.7\%}$	$439^{+9.8\%}_{-9.2\%}$	$487^{+8.4\%}_{-8.5\%}$	$498^{+8.1\%}_{-7.3\%}$
	$Q/2$	$468^{+9.8\%}_{-10.7\%}$	$477^{+8.6\%}_{-8.0\%}$	$498^{+6.1\%}_{-7.2\%}$	$499^{+6.5\%}_{-6.9\%}$
	$M/2$	$499^{+5.9\%}_{-9.3\%}$	$504^{+8.1\%}_{-7.8\%}$	$504^{+4.8\%}_{-6.1\%}$	$503^{+5.6\%}_{-6.7\%}$
14	Q	$506^{+11.8\%}_{-11.5\%}$	$530^{+9.8\%}_{-9.2\%}$	$588^{+8.5\%}_{-8.6\%}$	$601^{+8.1\%}_{-7.4\%}$
	$Q/2$	$566^{+9.9\%}_{-10.6\%}$	$576^{+8.7\%}_{-8.0\%}$	$601^{+6.3\%}_{-7.3\%}$	$602^{+6.5\%}_{-7.0\%}$
	$M/2$	$604^{+6.1\%}_{-9.2\%}$	$609^{+8.4\%}_{-7.8\%}$	$610^{+5.1\%}_{-6.2\%}$	$607^{+5.9\%}_{-6.8\%}$

Table 1. Total cross section predictions for the $pp \to t\bar{t}H$ at various LHC collision energies and central scale choices. The listed error is the theoretical error due to scale variation calculated using the 7-point method.

NLO+NNLL results show a remarkable stability w.r.t. the scale choice. We also observe that the 7-point method scale uncertainty of the results gets reduced with the increasing accuracy. In particular, for all scale choices, the scale uncertainty of NLO+NNLL cross section is reduced compared to the NLO scale uncertainty calculated in the same way. The degree up to which the scale uncertainty is reduced depends on the specific choice of the central scale. For example, for $\mu_0 = Q/2$ the theoretical precision of the NLO+NNLL prediction is improved by about 30% with respect to the NLO result, bringing the scale error calculated with the 7-point method down to less than 7% of the central cross section value. The results shown in Table 1 are further graphically presented in Fig. 2.

The size of the K_{NNLL} factor measuring the impact of the higher-order logarithmic corrections, defined as the ratio of the NLO+NNLL to NLO cross sections, is shown in Table 2. It varies depending on the value of the central scale. The variation is almost

2 around $\mu_0 = M/2$, while here we consider a much wider range between $M/2$ and Q.

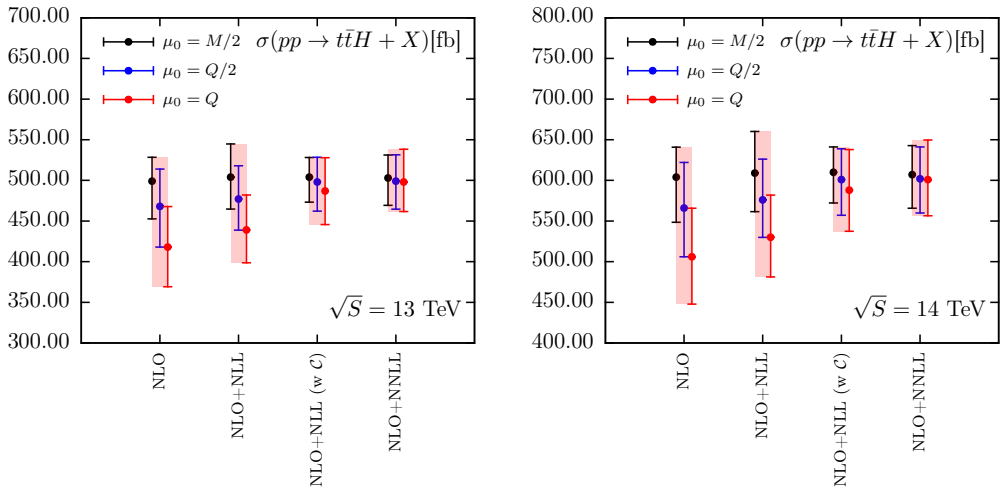

Figure 2. Graphical illustration of results presented in Table 1.

$\sqrt{S}$ [TeV]	μ_0	NLO+NNLL [fb]	$K_{\rm NNLL}$ factor
13	Q	$498^{+8.1\%+2.9\%}_{-7.3\%-2.9\%}$	1.19
	$Q/2$	$499^{+6.5\%+3.0\%}_{-6.9\%-3.0\%}$	1.07
	$M/2$	$503^{+5.6\%+3.1\%}_{-6.7\%-3.1\%}$	1.01
14	Q	$601^{+8.1\%+2.8\%}_{-7.4\%-2.8\%}$	1.19
	$Q/2$	$602^{+6.5\%+2.9\%}_{-7.0\%-2.9\%}$	1.06
	$M/2$	$607^{+5.9\%+3.0\%}_{-6.8\%-3.0\%}$	1.01

Table 2. Total cross section predictions at NLO+NNLL for the $pp \to t\bar{t}H$ at various LHC collision energies and central scale choices. The first error is the theoretical error due to scale variation calculated using the 7-point method and the second is the pdf error.

entirely driven by the scale dependence of the NLO cross section. For the choice $\mu_0 = Q$ the $K_{\rm NNLL}$-factor can be as high as 1.2.

Given the conspicuous stability of the NLO+NNLL results, see Fig. 2, we are encouraged to combine our results obtained for various scale choices. For this purpose we adopt the method proposed by the Higgs Cross Section Working Group [20]. In this way, we obtain for the $t\bar{t}H$ cross section at 13 TeV

$$\sigma_{\rm NLO+NNLL} = 500^{+7.6\%+3.0\%}_{-7.7\%-3.0\%} \text{ fb},$$

and at 14 TeV

$$\sigma_{\rm NLO+NNLL} = 603^{+7.7\%+2.9\%}_{-7.8\%-2.9\%} \text{ fb},$$

where the first error is the theoretical uncertainty due to scale variation and the second error is the pdf uncertainty.

Our findings are further illustrated in the plots in Fig. 3 and Fig. 4. We show there the scale dependence of $t\bar{t}H$ total cross sections calculated with the factorization and renormalization scale kept equal, $\mu = \mu_{\rm F} = \mu_{\rm R}$ for two LHC collision energies $\sqrt{S} = 13$ TeV and

$\sqrt{S} = 14$ TeV. As readily expected, apart from quantitative differences there is no visible disparity between the qualitative behaviour of results for the two energies. For the central scale choice of $\mu_0 = Q$, we observe a steady increase in the stability of the cross section value w.r.t. scale variation as the accuracy of resummation improves from NLO+NLL to NLO+NNLL. Our final NLO+NNLL prediction is characterised by a very low scale dependence if $\mu_F = \mu_R$ choice is made. Correspondingly, if calculated only along the $\mu_F = \mu_R$ direction, the theoretical error on the NLO+NNLL prediction due to scale variation would be at the level of 1%, which is a significant reduction from the 10% variation of the NLO, c.f. Table 1. Results obtained with the scale choice of $\mu_0 = M/2$ behave mostly in a similar way. Only in the very low scale regime, $\mu \lesssim 0.2M$, the NLO+NNLL cross section shows a stronger scale dependence. For this scale choice, the rise of the matched resummed predictions with the diminishing scale is driven by the fall of the expanded resummed NLL$|_{\rm NLO}$ results, cf. Fig.1, and a therefore is a consequence of the relatively large scale dependence of NLO contributions stemming from the qg channel.

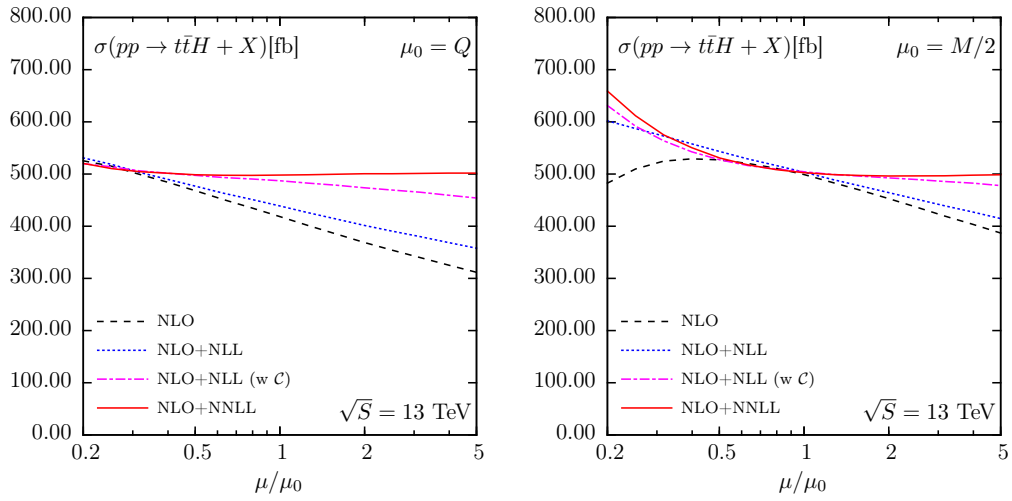

Figure 3. Scale dependence of the total cross section for the process $pp \to t\bar{t}H$ at the LHC with $\sqrt{S} = 13$ TeV. Results shown for the choice $\mu = \mu_F = \mu_R$ and two central scale values $\mu_0 = Q$ (left plot) and $\mu_0 = M/2$ (right plot).

We further investigate the dependence on the scale but showing separately the renormalization and factorization scale dependence while keeping the other scale fixed. Fig. 5 shows the dependence on μ_R and Fig. 6 on μ_F for the $\sqrt{S} = 14$ TeV. We conclude that the weak scale dependence present when the scales are varied simultaneously is a result of the opposite behaviour of the total cross section under μ_F and μ_R variations. The effect is similar to the cancellations between renormalization and factorization scale dependencies for threshold resummation in the absolute threshold limit which we observed in [23]. The typical decrease of the cross section with increasing μ_R originates from running of α_s. The behaviour under variation of the factorization scale, on the other hand, is related to the effect of scaling violation of pdfs at probed values of x. In this context, it is interesting to observe that the NLO+NLL predictions in Fig. 6 show very little μ_F dependence around

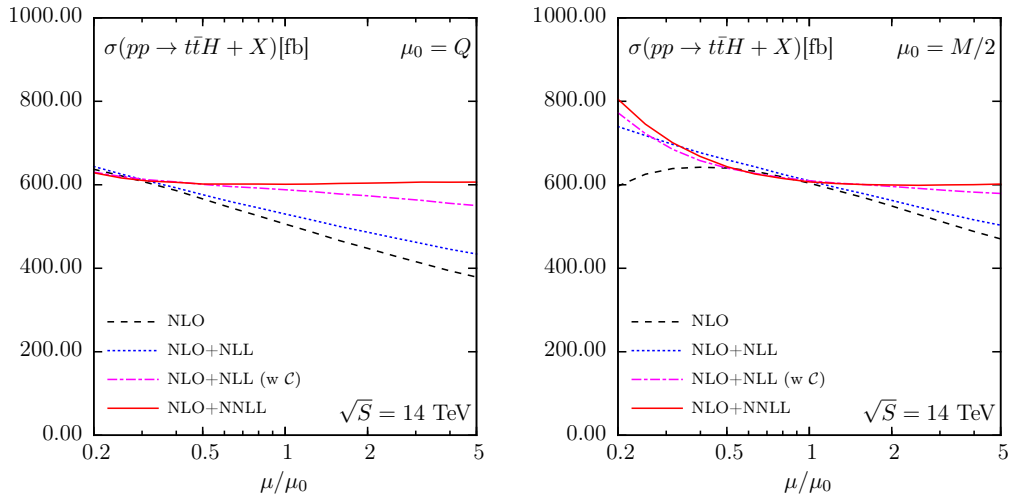

Figure 4. Scale dependence of the total cross section for the process $pp \to t\bar{t}H$ at the LHC with $\sqrt{S} = 14$ TeV. Results shown for the choice $\mu = \mu_{\rm F} = \mu_{\rm R}$ and two central scale values $\mu_0 = Q$ (left plot) and $\mu_0 = M/2$ (right plot).

the central scale, in agreement with expectation of the factorization scale dependence in the resummed exponential and in the pdfs cancelling each other, here up to NLL. The relatively strong dependence on $\mu_{\rm F}$ of the NLO+NLL predictions with non-zero $\mathcal{C}^{(1)}_{ij\to klB}$ can be then easily understood: the resummed expression will take into account higher order scale dependent terms which involve both $\mathcal{C}^{(1)}_{ij\to klB}$ and logarithms of N. These terms do not have their equivalent in the pdf evolution since the pdfs do not carry any process-specific information. Correspondingly, they are not cancelled and can lead to strong effects if the coefficients $\mathcal{C}^{(1)}_{ij\to klB}$ are numerically significant.

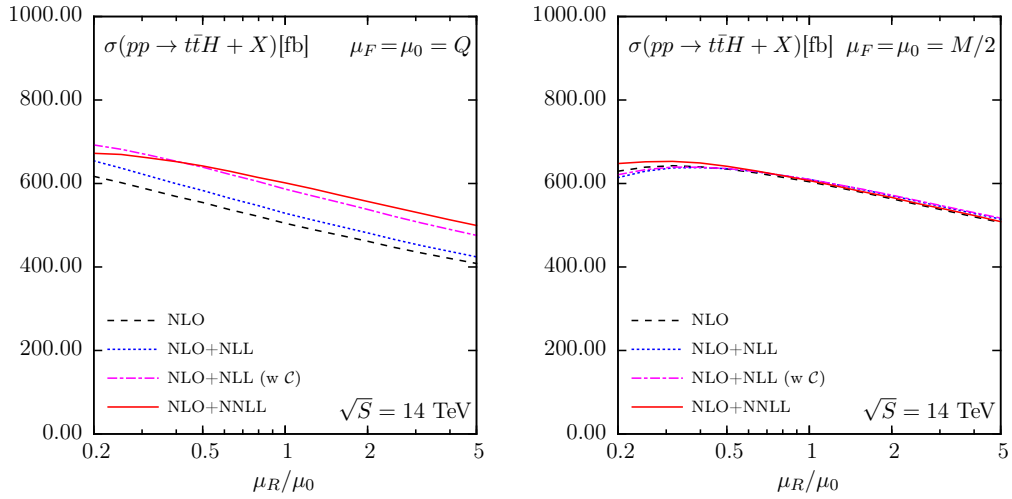

Figure 5. Renormalization scale dependence of the total cross section for the process $pp \to t\bar{t}H$ at the LHC with $\sqrt{S} = 14$ TeV and $\mu_{\rm F} = \mu_{\rm F,0}$ kept fixed. Results shown two central scale choces $\mu_0 = \mu_{\rm F,0} = \mu_{\rm R,0} = Q$ (left plot) and $\mu_0 = \mu_{\rm F,0} = \mu_{\rm R,0} = M/2$ (right plot).

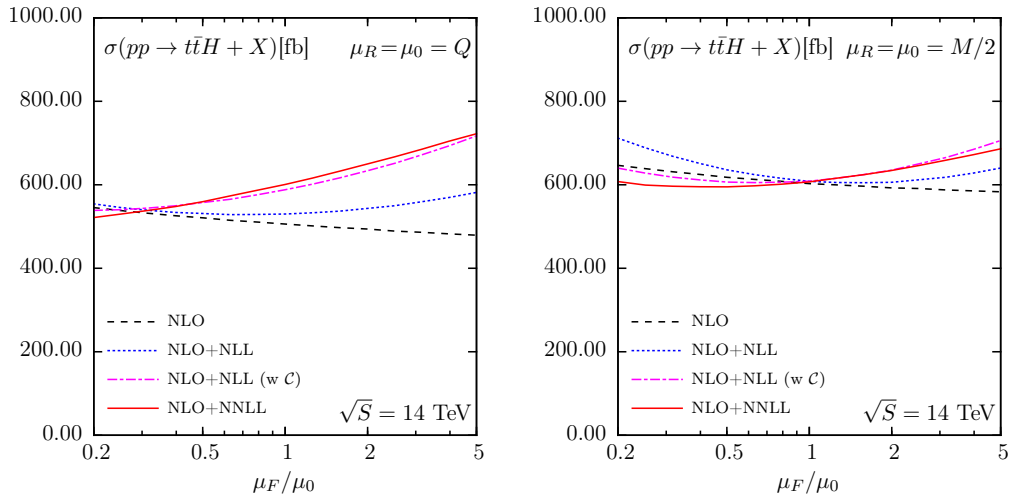

Figure 6. Factorization scale dependence of the total cross section for the process $pp \to t\bar{t}H$ at the LHC with $\sqrt{S} = 14$ TeV and $\mu_R = \mu_{R,0}$ kept fixed. Results shown two central scale choces $\mu_0 = \mu_{F,0} = \mu_{R,0} = Q$ (left plot) and $\mu_0 = \mu_{F,0} = \mu_{R,0} = M/2$ (right plot).

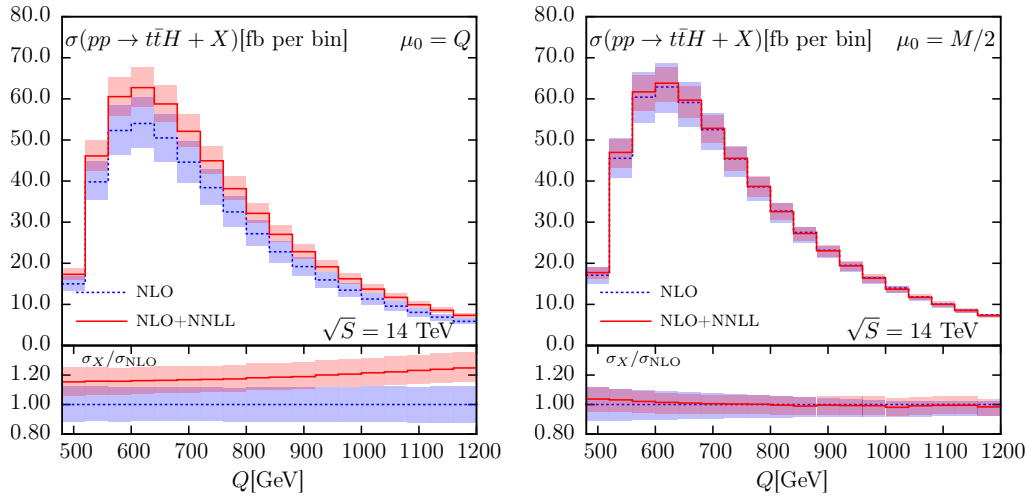

Figure 7. Comparison of the NLO+NNLL and NLO invariant mass distributions for the process $pp \to t\bar{t}H$ at the LHC with $\sqrt{S} = 14$ TeV. Results shown for two central scale choices $\mu_0 = Q$ (left plot) and $\mu_0 = M/2$ (right plot). Lower panels show the ratio of the distributions w.r.t. the NLO predictions.

Given apparent cancellations between $\mu_{\rm R}$ and $\mu_{\rm F}$ scale dependence, we believe that the 7-point method of estimating the scale error, allowing for an independent variation of $\mu_{\rm R}$ only (for $\mu_{\rm F} = \mu_0$), is better suited here as an estimate of the theory error than the often used variation of $\mu = \mu_{\rm F} = \mu_{\rm R}$. Another reason for our preference of this conservative estimate is presence of the hard-matching coefficients in the resummation formula, Eq. (2.15), which involve virtual corrections and are known only up to the order $\alpha_{\rm s}$. Due to suppression of the LO phase space, they provide a relatively significant part of the NLO+NNLL corrections to the total cross sections, cf. Table 1. It is then justified to suppose that a similar situation

might take place also at higher logarithmic orders and that the value of the yet unknown two-loop virtual correction which feeds into the second-order hard-matching coefficient can have a non-negligible impact on the predictions. With the 7-point method error estimate, we expect that this effect is included within the size of the error.

Our observation of stability of the predictions w.r.t. scale variation is also confirmed at the differential level. In Fig. 7 we show the differential distribution in the invariant mass Q of the $t\bar{t}H$ system produced at $\sqrt{S} = 14$ TeV. While the NLO distributions calculated with $\mu_0 = Q$ and $\mu_0 = M/2$ differ visibly, the NLO+NNLL distributions for these scale choices are very close in shape and value. The stability of the NLO+NNLL distribution w.r.t. the scale choice is demonstrated explicitly in Fig. 8. Correspondingly, the ratios of the NLO+NNLL to NLO distributions differ. In particular for the choice of $\mu_0 = Q$ the NNLL differential K-factor grows with the invariant mass and can be higher than 1.2 at large Q. The scale error for the invariant mass distribution is also calculated using the 7-point method. The error bands are slightly narrower for the NLO+NNLL distributions than at NLO. If the scale errors were calculated by variation of $\mu = \mu_F = \mu_R$ by factors of 0.5 and 2, the NLO+NNLL error bands would be considerably narrower.

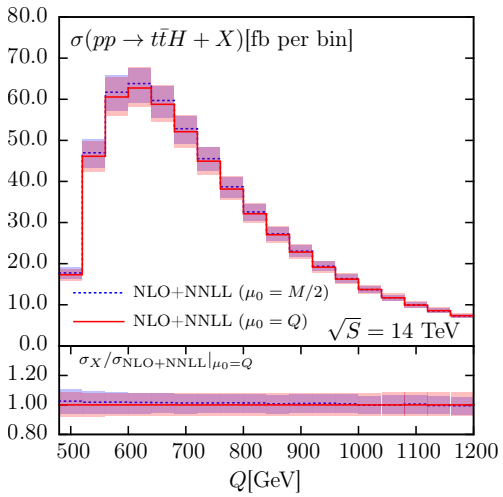

Figure 8. Comparison of the NLO+NNLL invariant mass distributions for the process $pp \to t\bar{t}H$ at the LHC with $\sqrt{S} = 14$ TeV calculated with $\mu_0 = Q$ and $\mu_0 = M/2$. Lower panel shows the ratio to the NLO+NNLL distribution with $\mu_0 = Q$.

We finish this discussion by comparing resummed results obtained using the invariant mass kinematics with those obtained earlier by us in the absolute mass threshold limit [23]. At 13 (14) TeV, our most accurate prediction in these kinematics, i.e. the NLO+NLL cross section including the first-order hard-matching coefficient, evaluated with PDF4LHC15_100 pdf sets, amounted to $\sigma_{\text{NLO+NLL w}\mathcal{C}} = 530^{+7.8\%}_{-5.5\%}$ $(641^{+7.9\%}_{-5.5\%})$. The absolute mass threshold approach allows only for a fixed scale choice, which is taken to be $\mu_0 = \mu_F = \mu_R = M/2$. Comparing this result with our NLO+NLL predictions for the same scale choice in the invariant mass kinematics, cf. Table 1, we see that the results calculated using the two resummation methods agree within errors.

4 Summary

In this work, we have investigated the impact of the soft gluon emission effects on the total cross section for the process $pp \to t\bar{t}H$ at the LHC. The resummation of soft gluon emission has been performed using the Mellin-moment resummation technique at the NLO+NNLL accuracy in the three particle invariant mass kinematics. We have considered the differential distribution in the invariant mass as well as the total cross section, obtained by integrating the distribution. Our NLO+NNLL predictions are very stable with respect to a choice of the central scale μ_0 for the invariant mass distribution, and consequently also for the total cross section. As this is not the case for the NLO predictions, the NNLL corrections vary in size, depending on the choice of the scale. In general, for the energies and scale choices considered they provide a non-negative modification of the cross section, which for the scale choice of $\mu_0 = Q$ can be even higher than 20% at larger values of Q^2.

We estimate the theoretical error due to scale variation by using the 7-point method, allowing for independent variation of renormalization and factorization scales. The overall size of the theoretical scale error becomes gradually smaller as the accuracy of resummation increases, albeit the reduction is relatively modest. The reduction would have been much more significant if the scale error had been estimated by simultaneous variation of renormalization and factorization scales, i.e. of $\mu = \mu_{\rm F} = \mu_{\rm R}$. However, as it seems that the reduction in this case is a result of cancellations between factorization and renormalization scale dependencies, we choose a more conservative 7-point approach for estimating the error.

The stability of NLO+NNLL results w.r.t. the scale choice allows us to derive our best prediction for the $pp \to t\bar{t}H$ total cross section at 13 TeV

$$\sigma_{\rm NLO+NNLL} = 500\,^{+7.6\%\,+3.0\%}_{-7.7\%\,-3.0\%}\ \text{fb},$$

and at 14 TeV

$$\sigma_{\rm NLO+NNLL} = 603\,^{+7.7\%\,+2.9\%}_{-7.8\%\,-2.9\%}\ \text{fb},$$

where the first error is the theoretical uncertainty due to scale variation and the second error is the pdf uncertainty. We note that the predictions are very close in their central value to the corresponding NLO predictions obtained for the scale choice $\mu_0 = M/2$ and are compatible with them within errors, vindicating the appropriatness of this commonly made choice. However, in comparison with the NLO predictions obtained in this way, our NLO+NNLL predictions are characterized by the overall smaller size of the theory error related to scale variation.

Note added: While this paper was being completed, Broggio *et al.* published independent results on soft gluon resummation for the $t\bar{t}H$ production process [28]. The authors of [28] use a resummation formula derived in the SCET framework in [26], though for the purpose of numerical calculations the Mellin space is adopted. Our results agree qualitatively with those in [28] regarding sensitivity of the size of NNLL corrections to the central scale choice, i.e. we also observe higher correction for the scale choice of $\mu_0 = \mu_{\rm F} = \mu_{\rm R} = Q$ than for

$\mu_0 = \mu_F = \mu_R = Q/2$. However, in contrast to [28], we find a remarkable stability of our final NLO+NNLL predictions for the total cross section, obtained for three various scale choices of $\mu_0 = M/2$, $\mu_0 = Q/2$ and $\mu_0 = Q$.

Acknowledgments

We are grateful to M. Krämer for providing us with a numerical code for NLO $t\bar{t}H$ cross section calculations [9]. This work has been supported in part by the DFG grant KU 3103/1. Support of the Polish National Science Centre grant no. DEC-2014/13/B/ST2/02486 is gratefully acknowledged. This work was also partially supported by the U.S. National Science Foundation, under grants PHY-0969510, the LHC Theory Initiative, PHY-1417317 and PHY-1619867. AK would like to thank the Theory Group at CERN, where part of this work was carried out, for its kind hospitality.

References

[1] G. Aad *et al.* [ATLAS Collaboration], Phys. Lett. B **740** (2015) 222 [arXiv:1409.3122 [hep-ex]].

[2] G. Aad *et al.* [ATLAS Collaboration], Eur. Phys. J. C **75** (2015) no.7, 349 [arXiv:1503.05066 [hep-ex]].

[3] V. Khachatryan *et al.* [CMS Collaboration], JHEP **1409** (2014) 087 [JHEP **1410** (2014) 106] [arXiv:1408.1682 [hep-ex]].

[4] V. Khachatryan *et al.* [CMS Collaboration], Eur. Phys. J. C **75** (2015) no.6, 251 [arXiv:1502.02485 [hep-ex]].

[5] G. Aad *et al.* [ATLAS Collaboration], Phys. Lett. B **749** (2015) 519 [arXiv:1506.05988 [hep-ex]].

[6] D. de Florian *et al.* [LHC Higgs Cross Section Working Group], arXiv:1610.07922 [hep-ph].

[7] The ATLAS collaboration [ATLAS Collaboration], ATLAS-CONF-2016-058, ATLAS-CONF-2016-067, ATLAS-CONF-2016-068, ATLAS-CONF-2016-080.

[8] CMS Collaboration [CMS Collaboration], CMS-PAS-HIG-15-008, CMS-PAS-HIG-16-004, CMS-PAS-HIG-16-020, CMS-PAS-HIG-16-022, CMS-PAS-HIG-16-038, CMS-PAS-HIG-17-004.

[9] W. Beenakker, S. Dittmaier, M. Krämer, B. Plumper, M. Spira and P. M. Zerwas, Phys. Rev. Lett. **87** (2001) 201805 [hep-ph/0107081]; W. Beenakker, S. Dittmaier, M. Krämer, B. Plumper, M. Spira and P. M. Zerwas, Nucl. Phys. B **653** (2003) 151 [hep-ph/0211352].

[10] L. Reina and S. Dawson, Phys. Rev. Lett. **87** (2001) 201804 [hep-ph/0107101]; L. Reina, S. Dawson and D. Wackeroth, Phys. Rev. D **65** (2002) 053017 [hep-ph/0109066]; S. Dawson, L. H. Orr, L. Reina and D. Wackeroth, Phys. Rev. D **67** (2003) 071503 [hep-ph/0211438]; S. Dawson, C. Jackson, L. H. Orr, L. Reina and D. Wackeroth, Phys. Rev. D **68** (2003) 034022 [hep-ph/0305087].

[11] V. Hirschi, R. Frederix, S. Frixione, M. V. Garzelli, F. Maltoni and R. Pittau, JHEP **1105** (2011) 044 [arXiv:1103.0621 [hep-ph]].

[12] R. Frederix, S. Frixione, V. Hirschi, F. Maltoni, R. Pittau and P. Torrielli, Phys. Lett. B **701** (2011) 427 [arXiv:1104.5613 [hep-ph]].

[13] M. V. Garzelli, A. Kardos, C. G. Papadopoulos and Z. Trocsanyi, Europhys. Lett. **96** (2011) 11001 [arXiv:1108.0387 [hep-ph]].

[14] H. B. Hartanto, B. Jager, L. Reina and D. Wackeroth, Phys. Rev. D **91** (2015) 9, 094003 [arXiv:1501.04498 [hep-ph]].

[15] S. Frixione, V. Hirschi, D. Pagani, H. S. Shao and M. Zaro, JHEP **1409** (2014) 065 [arXiv:1407.0823 [hep-ph]].

[16] S. Frixione, V. Hirschi, D. Pagani, H.-S. Shao and M. Zaro, JHEP **1506** (2015) 184 [arXiv:1504.03446 [hep-ph]].

[17] Y. Zhang, W. G. Ma, R. Y. Zhang, C. Chen and L. Guo, Phys. Lett. B **738** (2014) 1 [arXiv:1407.1110 [hep-ph]].

[18] A. Denner and R. Feger, JHEP **1511** (2015) 209 [arXiv:1506.07448 [hep-ph]].

[19] A. Denner, J. N. Lang, M. Pellen and S. Uccirati, JHEP **1702** (2017) 053 doi:10.1007/JHEP02(2017)053 [arXiv:1612.07138 [hep-ph]].

[20] S. Dittmaier *et al.* [LHC Higgs Cross Section Working Group Collaboration], arXiv:1101.0593 [hep-ph].

[21] R. Bonciani, S. Catani, M. L. Mangano and P. Nason, Phys. Lett. B **575** (2003) 268 [hep-ph/0307035].

[22] S. M. Aybat, L. J. Dixon and G. F. Sterman, Phys. Rev. Lett. **97** (2006) 072001 [hep-ph/0606254]; S. M. Aybat, L. J. Dixon and G. F. Sterman, Phys. Rev. D **74** (2006) 074004 [hep-ph/0607309].

[23] A. Kulesza, L. Motyka, T. Stebel and V. Theeuwes, JHEP **1603** (2016) 065 [arXiv:1509.02780 [hep-ph]].

[24] A. Kulesza, L. Motyka, T. Stebel and V. Theeuwes, arXiv:1609.01619 [hep-ph].

[25] H. T. Li, C. S. Li and S. A. Li, Phys. Rev. D **90** (2014) 9, 094009 [arXiv:1409.1460 [hep-ph]].

[26] A. Broggio, A. Ferroglia, B. D. Pecjak, A. Signer and L. L. Yang, JHEP **1603** (2016) 124 [arXiv:1510.01914 [hep-ph]].

[27] A. Broggio, A. Ferroglia, G. Ossola and B. D. Pecjak, JHEP **1609** (2016) 089 [arXiv:1607.05303 [hep-ph]].

[28] A. Broggio, A. Ferroglia, B. D. Pecjak and L. L. Yang, JHEP **1702** (2017) 126 [arXiv:1611.00049 [hep-ph]].

[29] A. Broggio, A. Ferroglia, G. Ossola, B. D. Pecjak and R. D. Sameshima, arXiv:1702.00800 [hep-ph].

[30] G. Sterman and M. Zeng, JHEP **1405** (2014) 132 [arXiv:1312.5397 [hep-ph]].

[31] N. Kidonakis, G. Oderda and G. Sterman, Nucl. Phys. B **531**, 365 (1998). [arXiv:hep-ph/9803241].

[32] H. Contopanagos, E. Laenen and G. F. Sterman, Nucl. Phys. B **484** (1997) 303 [hep-ph/9604313].

[33] M. Czakon, A. Mitov and G. F. Sterman, Phys. Rev. D **80** (2009) 074017 [arXiv:0907.1790 [hep-ph]].

[34] N. Kidonakis and G. Sterman, Nucl. Phys. B **505** (1997) 321 [arXiv:hep-ph/9705234].

[35] L. J. Dixon, L. Magnea and G. F. Sterman, JHEP **0808** (2008) 022 [arXiv:0805.3515 [hep-ph]].

[36] N. Kidonakis, G. Oderda and G. Sterman, Nucl. Phys. B **525**, 299 (1998) [arXiv:hep-ph/9801268].

[37] A. Ferroglia, M. Neubert, B. D. Pecjak and L. L. Yang, Phys. Rev. Lett. **103** (2009) 201601 [arXiv:0907.4791 [hep-ph]].

[38] A. Ferroglia, M. Neubert, B. D. Pecjak and L. L. Yang, JHEP **0911** (2009) 062 [arXiv:0908.3676 [hep-ph]].

[39] S. Catani, M. L. Mangano, P. Nason and L. Trentadue, Nucl. Phys. B **478**, 273 (1996) [arXiv:hep-ph/9604351].

[40] S. Catani, D. de Florian, M. Grazzini and P. Nason, JHEP **0307** (2003) 028 [hep-ph/0306211].

[41] A. J. Buras, Rev. Mod. Phys. **52** (1980) 199.

[42] V. Ahrens, A. Ferroglia, M. Neubert, B. D. Pecjak and L. L. Yang, JHEP **1009** (2010) 097 [arXiv:1003.5827 [hep-ph]].

[43] S. Catani, S. Dittmaier, M. H. Seymour and Z. Trocsanyi, Nucl. Phys. B **627** (2002) 189 [hep-ph/0201036].

[44] W. Beenakker, S. Brensing, M. Kramer, A. Kulesza, E. Laenen and I. Niessen, JHEP **1201** (2012) 076 [arXiv:1110.2446 [hep-ph]].

[45] W. Beenakker *et al.*, JHEP **1310** (2013) 120 [arXiv:1304.6354 [hep-ph]].

[46] R. Bonciani, S. Catani, M. L. Mangano and P. Nason, Nucl. Phys. B **529**, 424 (1998) [arXiv:hep-ph/9801375].

[47] J. Alwall *et al.*, JHEP **1407** (2014) 079 [arXiv:1405.0301 [hep-ph]].

[48] J. Butterworth *et al.*, J. Phys. G **43** (2016) 023001 [arXiv:1510.03865 [hep-ph]].